turns to its initial state. Rod B is used for vertical movements; heating this rod results in a lift of point P. All travel distances are increased by lever constructions to maximum values of 20 μm at the lever end.

When a slightly defocused laser beam (diameter ~50 μm) is scanned from right to left over rods A, B, and C, the freely movable horizontal rod R is moved ~5 μm to the right and placed back on the holders. Each cycle consists of the following steps: (i) Heating of rod A moves the lever to the left. (ii) Heating of rods A and B moves the lever up; rod R is lifted from the holders H and rests on the lever fork F. (iii) Heating of only rod B results in the return of rod R to the middle horizontal position. (iv) Heating of rods B and C moves the lever further to the right. (v) Heating of only rod C lowers the lever; rod R is placed back on the holders H, but the position is shifted to the right relative to the initial state. (vi) Cessation of heating of rod C restores the horizontal beginning position of the lever. The motor is now ready for a new cycle. Repeating the cycle results in longer distances of travel (Fig. 6).

The working principle of the micromotor resembles the contraction of a muscle through the interaction of myosin and actin (*12*). The maximum force the motor can apply is limited in this simple model by the adhesion of the horizontal bar to the fork during the movement. This adhesion force, ~10 nN, is on the order of the weight of the bar. If this adhesion is increased (for example, by a rougher surface), much higher values of the force—in the micronewton range, as calculated for the microtweezers—can be expected.

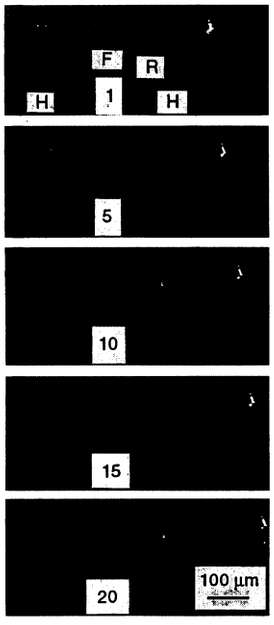

Fig. 6. Front view of the linear micromotor after 1, 5, 10, 15, and 20 cycles. The horizontal bar is moved ~100 μm to the right during 20 cycles (H, holders; F, fork; and R, rod).

The above examples suggest more complex applications for micromechanical devices fabricated by laser rapid prototyping from the gas phase. The one-step nature of the laser direct-write method makes structural evolution quick and easy, in contrast to mask-based processes. If focused laser light is used as the energy source, energy can easily be transferred to the moving structure; this would enable the creation of free "walking" devices with no mechanical connection to a battery or other energy source.

REFERENCES AND NOTES

1. T. M. Bloomstein and D. J. Ehrlich, *Appl. Phys. Lett.* **61**, 708 (1992); D. J. Ehrlich, *Appl. Surf. Sci.* **69**, 115 (1993).
2. F. T. Wallenberger, *Science* **267**, 1274 (1995).
3. D. Bäuerle, *Chemical Processing with Lasers* (Springer-Verlag, Heidelberg, 1987).
4. G. Leyendecker, D. Bäuerle, P. Geittner, H. Lydtin, *Appl. Phys. Lett.* **39**, 921 (1981).
5. D. Bäuerle, G. Leyendecker, D. Wagner, E. Bauser, Y. C. Lu, *Appl. Phys. A* **30**, 147 (1983).
6. F. T. Wallenberger and P. C. Nordine, *Science* **260**, 66 (1993).
7. P. C. Nordine, S. C. de la Veaux, F. T. Wallenberger, *Appl. Phys. A* **57**, 97 (1993).
8. F. T. Wallenberger and P. C. Nordine, *Mater. Lett.* **14**, 198 (1992).
9. M. Boman, H. Westberg, S. Johansson, J.-Å. Schweitz, *Proceedings of the 5th International Workshop on Micro Electro Mechanical Systems*, 4 to 7 February 1992, Travemünde, Germany (IEEE, Piscataway, NJ, 1992).
10. O. Lehmann and M. Stuke, *Mater. Lett.* **21**, 131 (1994).
11. *CRC Handbook of Chemistry and Physics* (CRC Press, Boca Raton, FL, ed. 61, 1981).
12. B. G. Levi, *Phys. Today* (April 1995), p. 17.

13. We thank K. Müller for expert technical assistance. Supported by Bundesministerium für Bildung, Wissenschaft, Forschung und Technologie grant 13N61597.

24 July 1995; accepted 16 October 1995

Defect Motion on an InP(110) Surface Observed with Noncontact Atomic Force Microscopy

Yasuhiro Sugawara, Masahiro Ohta, Hitoshi Ueyama, Seizo Morita

With an atomic force microscope operating in the noncontact mode in an ultrahigh vacuum, atomic-resolution imaging of the cleaved semi-insulating InP(110) surface has been achieved. By this method, atomic scale point defects and their motion were observed at room temperature, without the field-induced effects associated with scanning tunneling microscopy.

The ability to resolve individual atoms over a wide area makes the scanning tunneling microscope (STM) an excellent tool for studying the migration of atoms or defects. However, in all real-time STM experiments of surface dynamics processes, there is a high probability that the motion is nonthermal and is instead affected by the electric field or tunneling current; that is, the migration of the atoms or defects is the result of an excitation by the electric field of the biased tip or an energy injection by the tunneling current. It is well known that manipulation of single atoms is possible with the STM (*1*). Furthermore, STM tip–induced motion of the atoms or defects can exceed the thermal motion at room temperature (*2*, *3*). To investigate surface dynamics processes related to thermally induced motion of atoms or defects, one must remove tip-induced nonthermal motion.

The atomic force microscope (AFM) (*4*) is an alternative tool for high-resolution imaging. When operating in noncontact mode, it is expected to be free of such nonthermal effects and therefore to be effective for observing thermally induced motion in real time, because its operation is based on weak interactions attributable to attractive forces, rather than the electric field utilized in the STM. So far, the lateral resolution of noncontact ultrahigh-vacuum (UHV) AFM has been insufficient because of technical difficulties in measuring the weak distance dependence of the attractive forces between tip and sample, which have the high signal-to-noise ratio of the force measurements. Recently, the adatoms of the Si(111) 7×7 reconstructed surface were resolved locally by AFM, but stable imaging was not achieved (*5*). Furthermore, the distances between the adatoms and the corrugation heights with corner holes on the Si(111) 7×7 reconstructed surface are relatively large compared with those of other semiconductor surfaces. Continuing technical improvements increasing the lateral resolution of noncontact UHV AFM are required.

In this report, we present noncontact UHV-AFM images with atomic resolution for the semi-insulating InP(110) surface. Atomic scale point defects have been ob-

Department of Physics, Faculty of Science, Hiroshima University, 1-3-1 Kagamiyama, Higashi-Hiroshima, Hiroshima 739, Japan.

served at room temperature, and thermally induced motion of atoms or defects have been studied in real space.

We have used a very compact UHV AFM that allows in situ sample cleavage (6). The cantilever was scanned by a tube piezoelectric scanner, and its deflection was detected by an optical-fiber interferometer (7), which is one of the most sensitive displacement sensors. The frequency modulation (FM) detection method (8) was used to measure the force gradient acting on the tip. The tube piezoelectric scanner was also used to vibrate the cantilever at the mechanical resonant frequency. A positive feedback system with automatic gain control was used to maintain a constant vibration amplitude. The frequency shift of the cantilever was detected by a tunable analog FM demodulator.

As a force sensor, a silicon cantilever was used. When the attractive force gradient acting on the tip exceeds the spring constant of the cantilever, the cantilever jumps into the sample. Therefore, a stiff cantilever with a spring constant of $k = 34$ N/m and a mechanical resonant frequency of $\nu_0 = 151$ kHz was used to keep the cantilever from jumping and crushing the initially sharp tip. The sample was an Fe-doped semi-insulating InP(001) wafer (semi-insulating semiconductors cannot be studied by STM because of their lack of electrical conductivity). Sample cleavage and subsequent noncontact AFM measurements were performed at room temperature at pressures of less than 4×10^{-8} Pa. The images were obtained at constant force gradient; we kept the distance between the tip and the sample constant by maintaining a constant frequency shift $\Delta\nu$.

In an example of an actual image of a cleaved InP(110) surface by noncontact AFM (Fig. 1), the entire scan area is clearly resolved, including the rectangular lattice, which is slightly distorted as a result of thermal drift and creep of the piezoelectric micropositioners. In contact AFM imaging, the tip sticks to the sample at the beginning of the lateral scan (just after the lateral scan direction is reversed) because of static friction between tip and sample, and therefore, the observed atomic lattice periodicity is strongly distorted. In Fig. 1A, no such distortion occurs because noncontact imaging removes the friction effect between the tip and the sample surface.

The InP(110) surface is characterized by quasi–one-dimensional zigzag chains consisting of alternating In and P atoms (Fig. 1B) (2, 9). The electrons in the In dangling bonds partially transfer to the P, and the P atoms move out of the surface, resulting in a buckling. The lattice constants for the unit cell are 5.87 and 4.15 Å along the [001] and [1$\bar{1}$0] directions, respectively (2, 9). We have measured distances between the protrusions along the [001] and [1$\bar{1}$0] directions of 5.8 ± 0.6 and 4.3 ± 0.4 Å, respectively, in good agreement with the lengths for the unit cell. At present, we cannot clearly resolve the quasi–one-dimensional zigzag chains. The corrugation amplitudes were measured to be 0.19 ± 0.05 and 0.12 ± 0.05 Å along the [001] and [1$\bar{1}$0] directions, respectively. These amplitudes are about one-sixth of those obtained in contact-mode AFM (10). Note that the measured corrugation amplitudes depended on imaging parameters such as vibration amplitude A_0 and frequency shift $\Delta\nu$.

We have also been able to image atomic defects (Fig. 1A, feature a) reproducibly. Bright points on both sides of the atomic defects (features b and c) appear to be adsorbates. In Fig. 2, point defects are observed as atomic scale depressions (dark contrast) with respect to the background, suggesting that atoms have been removed from the surface. According to previous STM results (11) for the conducting InP(110) surface, these depressions may be "missing P defects" or "P vacancies"; we cannot verify the nature of the defects because the registry of the In and P sublattices is not resolved in the present AFM measurement. The defects may be caused by cleavage of the sample. The depressions observed in our measurements had approximate lateral dimensions of one unit cell in the [1$\bar{1}$0] direction, whereas vacancies observed with the STM broadened up to 4 nm as a result of the charge-induced band bending (2).

Occasionally, atomic scale point defects changed their relative position. In Fig. 2A, point defects d and e were separated by two atomic rows in the [001] direction. About 80 s later (Fig. 2B), defect e had split into two point defects, which were separated from defect d by three and four atomic rows, respectively, in the [001] direction; also, the distance between the point defects had decreased. Such position changes were studied for cases in which two or more defects were visible simultaneously; therefore, they do not reflect position changes of atoms on the tip apex because damage of the tip apex should affect all defects equally. The position change of the atomic scale point defects therefore originates from migration of the vacancies.

Our noncontact AFM observations show that vacancies can move not only within zigzag chains but also between zigzag chains. Experiments with a STM have

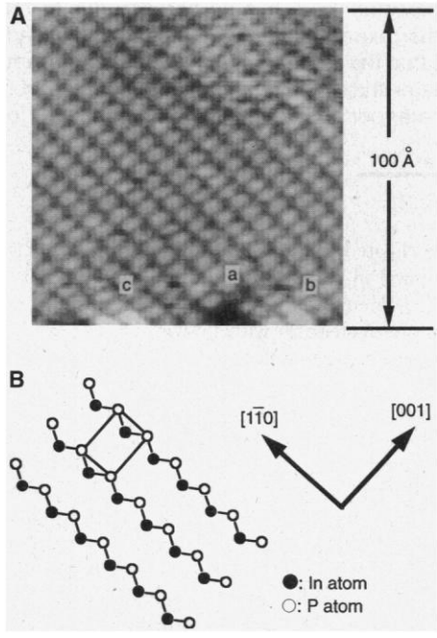

Fig. 1. (**A**) Noncontact UHV AFM image of the cleaved InP(110) surface. The scan area was 100 Å by 100 Å. Experimental conditions: spring constant of the cantilever $k = 34$ N/m, mechanical resonant frequency $\nu_0 = 151$ kHz, vibration amplitude $A_0 = 20$ nm, and frequency shift $\Delta\nu = -6$ Hz. Atomic defects (a) and adsorbates (b and c) are evident. (**B**) Surface structure of the InP(110) surface. The rectangle indicates a unit cell with lengths of 5.87 and 4.15 Å along the [001] and [1$\bar{1}$0] directions, respectively.

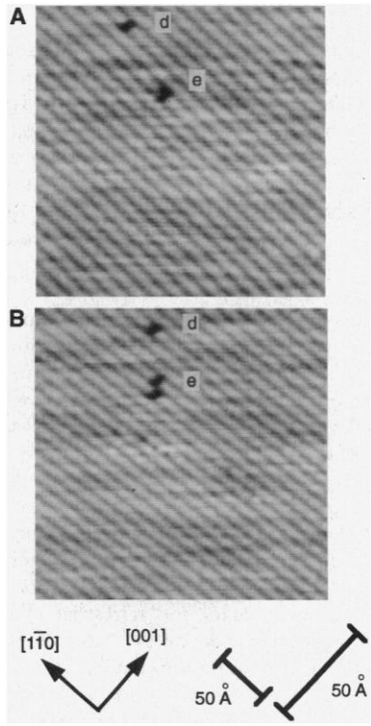

Fig. 2. Motion of atomic scale point defects. The fast scan direction was from left to right, and the slow scan direction was from bottom to top. (**A**) Point defects d and e are separated by two atomic rows in the [001] direction. (**B**) The same area imaged 80 s later. Defect e has split into two point defects, which are separated by three and four atomic rows, respectively, from defect d in the [001] direction. The distance between defects d and e has decreased.

shown that As vacancies on the GaAs(110) surface preferentially move between zigzag chains (*12*). This phenomenon can be understood in terms of simple bond-breaking and rebinding arguments (*12*). The observed migration of vacancies can be explained by the same arguments.

The motion of the defects could be thermally induced or the result of mechanical transfer of the atoms by the tip. In some cases, during the continuous observation of the same area, defects appeared and disappeared. The position changes were independent of the scanning direction, which indicates a thermal origin for the defect motion, but the present data is not sufficient to exclude other mechanisms. Quantitative comparison with STM imaging is necessary.

REFERENCES AND NOTES

1. D. M. Eigler and E. K. Schweizer, *Nature* **344**, 524 (1990); L. J. Whitman, J. A. Stroscio, R. A. Dragoset, R. J. Celotta, *Science* **251**, 1206 (1991); I.-W. Lyo and Ph. Avouris, *ibid.* **253**, 173 (1991).
2. Ph. Ebert, G. Cox, U. Poppe, K. Urban, *Ultramicroscopy* **42–44**, 871 (1992).
3. Ph. Ebert, M. G. Lagally, K. Urban, *Phys. Rev. Lett.* **70**, 1437 (1993).
4. G. Binnig, C. F. Quate, Ch. Gerber, *ibid.* **56**, 930 (1986).
5. F. J. Giessibl, *Science* **267**, 68 (1995); S. Kitamura and M. Iwatsuki, *Jpn. J. Appl. Phys.* **34**, L145 (1995).
6. M. Ohta *et al.*, *J. Vac. Sci. Technol. B* **12**, 1705 (1994).
7. D. Rugar, H. J. Mamin, P. Guethner, *Appl. Phys. Lett.* **55**, 2588 (1989).
8. T. R. Albrecht, P. Grütter, D. Horne, D. Rugar, *J. Appl. Phys.* **69**, 668 (1991).
9. R. J. Meyer *et al.*, *Phys. Rev. B* **22**, 6171 (1980).
10. M. Ohta *et al.*, *J. Vac. Sci. Technol. B* **13**, 1265 (1995).
11. Ph. Ebert, K. Urban, M. G. Lagally, *Phys. Rev. Lett.* **72**, 840 (1994).
12. G. Lengel, M. Weimer, J. Gryko, R. E. Allen, *J. Vac. Sci. Technol. A* **12**, 1855 (1994).

13. We thank F. Osaka and S. Ohkouchi of Optoelectronics Technology Research Laboratory and M. Suzuki of Nippon Telegram and Telephone Interdisciplinary Research Laboratories for valuable discussions. We thank S. Mishima of Olympus Optical for technical support. M.O. is a Research Fellow of the Japan Society for the Promotion of Science. Part of this work was supported by a Grant-in-Aid for Scientific Research from the Ministry of Education, Science, and Culture.

27 July 1995; accepted 11 October 1995

Behavior of the Heliosphere over Prolonged Solar Quiet Periods by ^{44}Ti Measurements in Meteorites

G. Bonino,* G. Cini Castagnoli, N. Bhandari, C. Taricco

The heliospheric magnetic field (HMF) is controlled by solar activity, as established by measurements over the last few decades, but its characteristics when the sun was quiet for prolonged periods, such as during Gleissberg or Maunder minima, are not known. Titanium-44, produced in meteorites, provides a monitor of the galactic cosmic ray (GCR) flux and allows estimation of the modulation effect of the sun for the period 1883 to 1992. The titanium-44 activity is consistent with the expected value, but the increase, due to the last Gleissberg minimum, is four times greater than expected for a GCR modulation based solely on sunspot numbers. This result implies that the HMF was weaker than at present and as a result the GCR flux (for energy greater than 1 gigaelectron volt) was higher between 2.2 to 3.6 protons per square centimeter per second per 4π steradians at 1 to 3 astronomical units in solar cycles 12 to 15.

Production of cosmogenic radioisotopes in meteorites depends on the GCR flux, which is controlled by the HMF which, in turn, depends on solar activity. GCR flux is inversely correlated with sunspot number. The radioisotopes can, therefore, serve as proxy records of solar activity. This approach has been used to understand solar behavior in the past based on records from terrestrial archives, such as ^{14}C in tree rings (*1*) and ^{10}Be in ice cores (*2*) and sediments, but such records are not free from interference of the terrestrial climate that governs the deposition rates of these isotopes in various terrestrial reservoirs (*1*). A similar approach, that of using isotopes produced in meteorites, offers a direct assessment of the solar activity, free from the influence of climatic cycles on Earth. The effect of the 11-year solar cycle has been quantitatively estimated by analysis of ^{22}Na (half-life, 2.6 years) in meteorites (*3*, *4*) and lunar samples (*5*). Here we use measurements of ^{44}Ti in stone meteorites with known dates of fall to assess century-scale variations in GCR flux.

^{44}Ti has a mean life of about 96 years (*6*) and is thus ideal for monitoring the behavior of the sun during the past 100 or 200 years. It is produced in cosmic-ray interactions (>70 MeV) in meteoritic iron and nickel (*7*). Attempts to determine its variation by radiochemical separation in several meteorites have not yielded measurable activity (*8*) because its production cross section is low, resulting in ^{44}Ti activity of about 1 dpm per kilogram of chondrite. We have therefore designed (*9*) a sensitive and selective γ-ray spectrometer to measure activity of its daughter, ^{44}Sc (half-life, 3.93 hours), which is in secular equilibrium with its parent, ^{44}Ti. ^{44}Sc decays by β^+ emission in coincidence with a 1157-keV γ-ray. Interference from the ubiquitous, naturally occurring ^{214}Bi (1155 keV) can be suppressed when the Ge detector is used in coincidence with a surrounding NaI(T) detector that operates only in annihilation γ-ray windows. By situating the spectrometer at an equivalent water depth of 70 m under Monte dei Cappuccini in Torino in a nitrogen atmosphere, a background of ~0.6 counts per day in 1157-keV channels was achieved.

We counted 10 fragments of nine chondrites: Alfianello (L6, 625 g), Lancon (H6, 1080 g), Holbrook (L6, 331 g), Olivenza (LL5, 247 g), Rio Negro (L4, 388 g), Monze (L6, 165 g), Dhajala (H3, 700 g), Torino (H6, 445 g), and Mbale (L5/6, 700 and 730 g) that fell during the period 1883 to 1992. The activity of ^{26}Al (1809 keV), ^{40}K (1461 keV), and ^{44}Ti (^{44}Sc, 1157 keV) was measured by counting fragments for a period

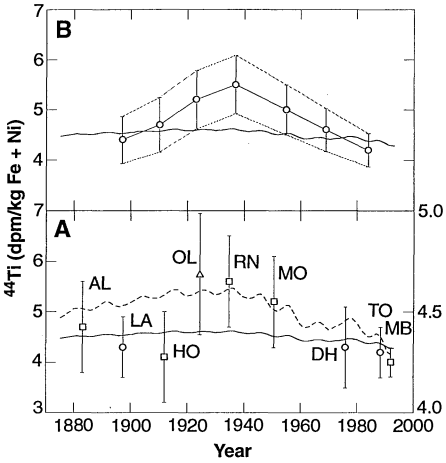

Fig. 1. (**A**) Observed ^{44}Ti activity (dpm per kilogram of Fe + Ni) for H (○), L (□), and LL (△) chondrites. AL, Alfianello; LA, Lancon; HO, Holbrook; OL, Olivenza; RN, Rio Negro; MO, Monze; DH, Dhajala T273; TO, Torino; MB, Mbale-T and Mbale-A. The variation expected due to modulation of GCR by sunspot activity is shown by a thick curve and, on a magnified (right hand) scale, by a dashed curve to illustrate small variations expected due to the Schwabe cycles. (**B**) Comparison of the three-point running mean and the error on the trend (dotted curve) with the expected profile based on the sunspot numbers.

G. Bonino, G. Cini Castagnoli, C. Taricco, Istituto di Cosmogeofisica, Corso Fiume 4, 10133 Torino, Italy, and Istituto di Fisica Generale dell'Universita', Via Giuria 1, 10125 Torino, Italy.
N. Bhandari, Physical Research Laboratory, Ahmedabad 380009, India.